M&C 2017 - International Conference on Mathematics & Computational Methods Applied to Nuclear Science & Engineering, Jeju, Korea, April 16-20, 2017, on USB (2017)

Quantification of ATF Concept Assessment Factors Using Multiphysics Simulations

James B. Tompkins,* Ryan G. McClarren,* Jason D. Hales †

*Department of Nuclear Engineering, Texas A&M University, 3133 TAMU, College Station, TX 77843
†Fuels Modeling & Simulation, Idaho National Laboratory, 2525 N. Fremont Ave., Idaho Falls, ID 83415
tompkins@tamu.edu, rgm@tamu.edu, jason.hales@inl.gov

Abstract - *In persuit of a quantitative method of comparing accident tolerant fuel concepts to traditional fuel behaviors, a method of applying failure probabilities in an existing fuel assessment framework is proposed. To demonstrate this process, an example case is undertaken by utilizing coupled multiphysics codes to investigate uranium silicide and uranium oxide fuel behaviors during a postulated reactivity insertion accident. An upper limit on each fuel system's surface cladding temperature is used to classify pass and fail cases on perturbed simulations. Sensitivity analysis reduces the dimensionality of the problem and a global geometric classification method predicts the limit surface separating pass and fail cases in the hyperspace made up of sensitive input variables. Numerically integrating this surface yields the probability of failure of the fuel concepts. Results demonstrate the method's viability as a fuel evaluation technique, but ongoing work will allow for quantification of proposed concept assessment factors.*

I. INTRODUCTION

In the wake of events at Fukushima Daiichi in 2011, there has been renewed worldwide interest in the development of nuclear fuel with greater tolerance for safe operation in accident conditions. Recent collaborative efforts between laboratories, industry, and universities to develop accident tolerant fuels (ATF) have produced numerous concepts, and an aggressive ATF implementation schedule has yielded several candidate materials with promising experimental results. Physical investigation alone, though, cannot provide the extensive data necessary for a thorough assessment. To aid in the analysis of ATF concepts, the Nuclear Energy Advanced Modeling & Simulation (NEAMS) program has directed a High Impact Problem aimed at supporting the Advanced Fuels Campaign by utilizing multiscale, multiphysics fuel performance modeling and simulations capabilities [1]. By employing state-of-the-art computational tools in ATF appraisals, more complete insights into fuel concepts' behaviors are gained.

Results from advanced analyses of ATF concepts are not directly comparable with traditional fuels' performance metrics as the new materials are designed to react to system transients differently. A method of accurately comparing fuel behaviors and drawing conclusions about the advantages and disadvantages of each fuel system should utilize results from both fuels under similar reactor system conditions while accomodating differences in fuel designs. Using a developed evaluation framework, we propose a methodology to calculate Concept Assessment Factors (CAFs), providing a numeric score for ATF candidate reviewers to consider in their appraisals. Simulations of silicide and oxide fuel elements during a reactivity insertion accident (RIA) serve as an example to demonstrate the methodology. Models from BISON coupled to RELAP-7 provide thermomechanical and two-phase thermohydraulic results for the posed problem, and model input variables are perturbed to investigate sensitivity of parameters as well as determine a hypersurface separating pass and fail cases. The failure probability of each fuel system can then be calculated and a comparison will yield a quantitatively determined Concept Assessment Factor.

II. THEORY AND CONTRIBUTING WORK

The following framework employed to assess ATF concepts already details methods an evaluator might use to determine the strengths of various fuel systems, but the base metrics are determined subjectively. In order to reduce the framework's reliance upon qualitatively determined metrics, the addition of factors arrived at through multiphysics simulation results is presented. An overview of the technical performance evaluation framework as well as a description of the demonstration problem to illustrate CAF quantification are specifed in this section. The tools utilized to solve the demonstration problem are also outlined with a brief accounting of the methods utilized in these codes and physical quantities able to be modeled. Lastly, one may find a summary of statistical and machine learning methods employed in quantification of CAFs in this section.

1. Concept Assessment Framework

To quantitatively determine the viability of ATF concepts, a method of evaluating advanced fuel candidates in a variety of operational conditions was developed by Bragg-Sitton et al. [2]. The methodology outlines methods of evaluation in three phases of technological development: Feasibility Assessment (proof-of-concept), Development and Qualification (proof-of-principle), and Commercialization (proof-of-performance) [2]. At any stage of investigation a Candidate Fuel System Attributes Assessment Table is used to evaluate fuel system concepts [2]. This table divides attributes into Performance Regimes including fabrication, normal operation, design basis accidents, severe accidents, and fuel storage with associated regime ranks and weights in ascending order of perceived importance [2]. Each regime is further divided into Performance Attributes representing behaviors and interactions necessary to consider in that Performance Regime with each attribute having an associated rank and weight [2]. The attributes are in-

dividually compared between the concept and traditional UO_2-zircaloy fuel system to obtain Concept Assessment Metrics (CAMs) that contribute to benefits and vulnerabilities separately [2]. Assessment scores for candidate fuel systems are determined for benefits and vulnerabilities by summing the weighted CAMs:

$$Score_{Benefit} = \sum_{i=1}^{V} w_i \sum_{j=a}^{h} w_j CAM_{Benefit} \tag{1a}$$

and

$$Score_{Vulnerability} = \sum_{i=1}^{V} w_i \sum_{j=a}^{h} w_j CAM_{Vulnerability}\,, \tag{1b}$$

where w_i is the fractional regime weighting and w_j is the attribute weight within the regime [2]. The weighting factors listed in the developed table were determined with input from academic and industry professionals [2]. While the work makes a point of determining the CAMs subjectively, we propose using advanced simulation capabilities to quantify Concept Assessment Factors (CAFs) that fit into the technical performance evaluation framework in place of the subjective metrics [2].

2. Concept Assessment Factor Quantification

The projected workflow for quantifying Concept Assessment Factors is shown in Figure 1. Diamond shaped nodes in this figure denote decisions to be made at the beginning of the CAF quantification process. Each decision limits further evaluation choices until some physical parameter(s) contributing to quantification of a performance attribute and a failure condition for the parameter are determined. After first selecting a candidate fuel system to investigate, one then chooses the regime in which the system operates in the simulation. A performance attribute aiding in evaluating the operation regime is next selected from attribute assessment table Identifiers. The multiphysics capabilities of the tools selected determine both the operation regimes and performance attributes able to be modeled, thus the tools selected largely determine the CAFs that can be computed. Physical properties prominently influencing the chosen performance attribute are selected from quantities the computational tools are able to model, and a failure criterion for physical properties can be determined from either an actual limit (e.g. boiling point for fluid temperature) or safety factor on a quantity limit. In addition to nominal material properties required to model the variable of interest in the operation regime chosen, distributions for these input variables in the computational tools are necessary to perform the sensitivity and classification analyses to quantify CAFs.

A demonstration case is undertaken to demonstrate this process. Employing coupled BISON and RELAP-7 simulations to solve fuel element thermomechanics and coolant channel thermal hydraulics allows for a wide range of CAFs to be quantified as the coupled codes are able to model myriad physical parameters affecting performance attributes of interest in several operation regimes. In addition to traditional fuel concepts, BISON has already implemented thermomechanical, material, and behavioral models for ATF concepts such as FeCrAl alloy cladding and silicide fuels [3]. Subsection **II. 3.** Computational Tools contains descriptions and overviews of the capabilities for these tools; the remainder of this section is devoted to characterizing the demonstration case chosen to quantify a CAF.

A case must be chosen for a concept with methods already implemented in operating regimes of interest in the selected tools. An assessment of the uranium silicide (U_3Si_2) fuel concept during a reactivity insertion accident is both a novel problem which coupled BISON and RELAP-7 can solve and serves to evaluate a CAF for the thermal behavior of U_3Si_2 in the postulated accident regime. Numerous quantities of interest are available to compare oxide and silicide thermal behavior performance, but to limit the focus of the demonstration case, the maximum outer cladding temperature is chosen. A failure condition of 1140 K on the outer surface of the cladding allows for a 0.45 safety factor on the melting temperature of zircaloy and corresponds to the middle of the elastic modulus' interpolation temperature evaluation range [4].

Simulating a single 4.435 meter PWR reactor fuel element and coolant channel, the system starts up to a low power, steady state condition after which the RIA occurs and the system recovers. The power history during the RIA is derived from scaled experimental control rod ejection data in a Brookhaven National Laboratory report (see Figure 2) [5]. The power profiles with which each fuel is simulated are shown in Figure 2. The differing power profiles are necessary to obtain the same nominal maximum outer cladding temperature of approximately 1130 K, but initial results are also compared with UO_2 results with the same power profile of the silicide fuel.

To perform sensitivity analysis and perturb input variables to create a limit surface, distributions for the variables need to be specified and sampled. Parameter distributions from the Phase-II OECD NEA RIA fuel codes benchmark are employed in this analysis (Table I) [6]. Variables include pressures, velocities, temperatures, densities, physical measurements, and scaling factors for thermal parameters ($f_{k,\text{fuel}}$, $f_{k,\text{clad}}$, $f_{c_p,\text{fuel}}$).

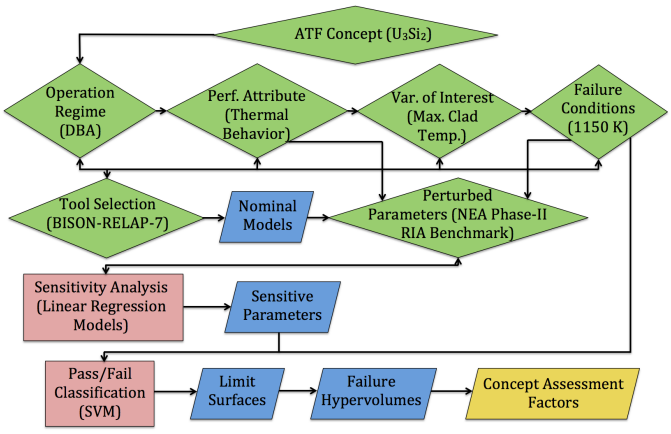

Fig. 1. Proposed workflow to quantify CAFs. Selection of demonstration problem characteristics are in parentheses.

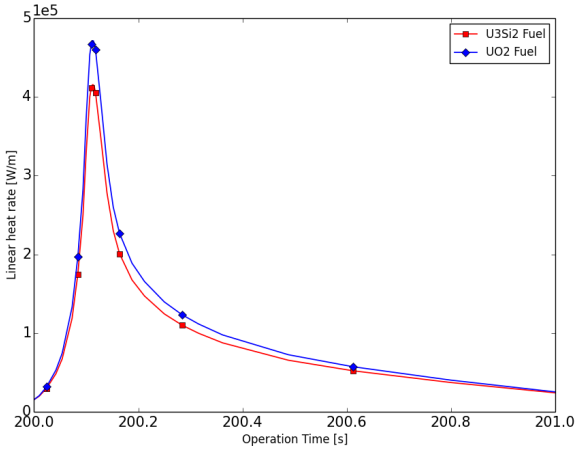

Fig. 2. Linear heat rate provided as a power history to BISON during the RIA.

Parameter	Unit	Mean	Std. Dev.
$p_{\text{liq.,init.}}$	Pa	15.5×10^6	0.075×10^6
$v_{\text{liq.,init.}}$	m/s	4.00	0.04
$T_{\text{liq.,init}}$	K	280	1.5
ρ_{fuel}	kg/m^3	10431.0	51.5
$d_{\text{clad\_out}}$	m	9.4×10^{-3}	0.01×10^{-3}
$d_{\text{clad\_in}}$	m	8.26×10^{-3}	0.01×10^{-3}
$p_{\text{plen.,init.}}$	Pa	2.0×10^6	0.05×10^6
R_{clad}	m	0.5×10^{-6}	0.25×10^{-6}
R_{fuel}	m	2.0×10^{-6}	1.0×10^{-6}
$f_{k,\text{fuel}}$	-	1.0	0.05
$f_{c_p,\text{fuel}}$	-	1.0	0.05
$f_{k,\text{clad}}$	-	1.0	0.015

TABLE I. Distributions for parameters to perturb for RIA [6].

3. Computational Tools

Figure 1 demonstrates the necessity of selecting appropriate computational tools. Codes utilized to simulate fuel behaviors need to be able to accurately simulate fuel concept responses in various operation regimes and calculate parameters affecting chosen performance attributes of interest while being robust enough to simulate failure conditions. Coupled BISON and RELAP-7 calculations meet all of the above requirements and perturbed models from RAVEN give insights into simulation uncertainties. With RAVEN driven BISON and RELAP-7 simulations, Concept Assessment Factors are able to be quantified.

One of NEAMS' tools of choice for fuel performance modeling is Idaho National Laboratory's (INL) BISON code which integrates developed nuclear material and behavioral models in the heat transfer and solid mechanics modules available in the MOOSE finite element framework on fuel element meshes to effectively model fuel system thermomechanics [3]. In addition to traditional fuel concepts, BISON has already implemented thermomechanical, material, and behavioral models for ATF concepts such as FeCrAl alloy cladding and silicide fuels [3]. The developed BISON models for both fuel cases contain methods for fuel and cladding solid mechanics, heat transfer , thermal and mechanical contact, and plasticity clad models. As BISON has been developed using the MOOSE framework, it can be easily coupled with other codes developed in the framework provided the physics they model are able to be employed as a boundary condition or source in BISON models to extend its multiphysics capabilities [7].

RELAP-7, an INL development code for thermal hydraulics built on the MOOSE framework, can be coupled to BISON through the MAMMOTH application to calculate coolant channel conditions during simulated reactor operations and pass temperature and pressure to the models in BISON as a boundary condition [7] [8]. RELAP-7 simulations use a seven equation, two-phase fluid flow model with various stabilization techniques and have integrated probabilistic risk assessment capabilties [8]. Our coupled simulation uses control logic to vary coolant inlet velocity and density as the system starts up, and the entropy viscosity method is employed for stabilization. While BISON does have a coolant channel model capable of calculating heat transfer from the outer clad wall into the coolant, it is only able to simulate thermal energy deposition in the coolant during steady state and slow operating transient conditions facilitating the choice of the coupled simulation for a RIA [3]. By coupling to RELAP-7, the thermal hydraulic simulation response capabilities are greatly expanded in BISON models, especially in fast transient cases such as a RIA.

Coupling these codes enables modeling of fuel elements and coolant channel response during operational transients using thermomechanical and thermal hydraulics methods to simulate a fuel system's behavior, but neither on their own allow a user to perturb input variables, necessary when exploring output response to predictors. RAVEN allows users to provide distributions for input variables from which it can then sample for use in generated input files for perturbed code runs [9]. Its capabilities include scheduling multiple jobs to run in parallel and constructing statistical models from collected output for a variety of analyses [9]. Developed statistical modeling capabilities are supplemented by the scikit-learn Python machine learning module which is employed in this work for its linear regression models used to perform sensitivity analysis [9]. In addition, RAVEN's adaptive sampler is used to determine the limit surface separating pass and failure states by utilizing support vector machines (SVM), a geometric classification method [9].

4. Statistical & Machine Learning Methods

The linear model fit with the least squares method could be called the most ubiquitous paradigm in the zeitgeist of contemporary statistics. Making large assumptions about the structure of predictive solutions, the linear model yields stable solutions applicable to a a great number of datasets [10]. The output Y of a model is predicted from a provided vector of inputs $X^T = \left(X_1, X_2, \ldots, X_p\right)$ via

$$\hat{Y} = \hat{\beta}_0 + \sum_{j=1}^{p} X_j \hat{\beta}_j \,, \tag{2}$$

where the term $\hat{\beta}_0$ is the intercept [10]. In order to fit the model to training data, the coefficients β are chosen to minimize the residual sum of squares

$$\hat{\beta} = \underset{\beta}{\operatorname{argmin}} \left\{ \sum_{i=1}^{N} (y_i - \beta_0 - \sum_{j=1}^{p} x_{ij}\beta_j)^2 \right\} \text{ [10].} \quad (3)$$

The residual sum of squares' minimum always exists (as it is a quadratic function), but this minimum may not be unique [10]. By imposing penalties on the size of least squares coefficient estimates, shrinkage methods arise. Ridge regression applies a sum-of-squares (L_2) penalty to the coefficients

$$\hat{\beta}^{\text{ridge}} = \underset{\beta}{\operatorname{argmin}} \left\{ \sum_{i=1}^{N} (y_i - \beta_0 - \sum_{j=1}^{p} x_{ij}\beta_j)^2 + \lambda \sum_{j=1}^{p} \beta_j^2 \right\} \quad (4)$$

which shrinks β values both towards zero and other coefficients, alleviating the high variance of linear regression models with many correlated variables [10]. The complexity parameter $\lambda \geq 0$ determines the amount of shrinkage applied to the coefficients [10]. Next, the lasso's coefficient estimation is given by

$$\hat{\beta}^{\text{lasso}} = \underset{\beta}{\operatorname{argmin}} \left\{ \frac{1}{2} \sum_{i=1}^{N} (y_i - \beta_0 - \sum_{j=1}^{p} x_{ij}\beta_j)^2 + \lambda \sum_{j=1}^{p} |\beta_j| \right\} \quad (5)$$

where again, the $\lambda \geq 0$ is the complexity parameter used to vary shrinkage [10]. Notice that the L_2 penalty $\sum_1^p \beta_j^2$ from ridge regresssion is now an L_1 sum of absolute values penalty $\sum_1^p |\beta_j|$ for the lasso [10]. The absolute value contraint causes some coefficients to be exactly zero for large λ's living up to its name by "lassoing" sensitive parameters, thus selecting a subset of input variables [10]. The elastic net penalty is a compromise between the lasso penalty's indifference to the choice among a set of sensitive but correlated variables and the ridge penalty's tendency to shrink the coefficients of correlated variables toward one another

$$\sum_{j=1}^{p} \left(\alpha|\beta_j| + (1-\alpha)\beta_j^2 \right) \quad (6)$$

where α is a parameter that determines the weights of the penalties [10].

One challenge in utilizing shrinkage methods to build predictive models is the selection of complexity and weighting parameters. The values of these parameters yielding the best fit can be determined via cross-validation, leaving a portion of the data out when training models then using the left out data to test the accuracy of the resultant model by comparing prediction values with the quantity of interest and iteratively determining the penalties that reduce model error by the greatest amount [10].

How then is the training data obtained? Looking back to Figure 1, the perturbed parameters chosen as input for the nominal models feed into the sensitivity analysis. However, generating models with the perturbed parameters is a problem of scale: each data point obtained is computationally expensive, but model error is reduced by exploring a greater amount of the sample space. To sample a variety of input values while being conservative with computational resources, the sampling scheme utilized is the latin hypercube, a grid based approach in which each sample is individually limited to one axis-aligned hyperplane [11]. A major advantage of this method is the independence of the number of samples upon the number of inputs to explore [11].

After training the models, the sensitivity of chosen output parameters to input variables can be determined from the model coefficients. The coefficients produced weight how important each associated input variable is in predicting output, but the coefficients must be converted to the same units before being compared. By multiplying coefficients by their associated variables' sample distribution parameters, the unitless coefficients rank, in descending magnitude, input variables having the greatest effect upon the model's output.

With sensitive parameters identified and a failure condition available, support vector machines (SVM) can be used to find a limit surface for the classification problem. The goal is to determine the hypersurface in a subset of sensitive parameters separating pass and fail cases determined by the parameter of interest's failure condition. The most important parameters identified in the sensitivity analysis can be used as a subset selection of perturbed input variables to minimize the amount of sample data required to accurately identify input behaviors affecting the quantity of interest. To find a limit surface, support vector classifiers, a global geometric classification method, find maximum margin hyperplanes by constructing lines from a set of points [10]. These lines are then used to determine a limit surface via an optimization scheme

$$\min_{\beta,\beta_0} \|\beta\| \quad (7)$$
$$\text{subject to } y_i(x_i^T\beta + \beta_0) \geq 1, i = 1, \ldots, N \text{ [10].}$$

This method can be extended to use nonlinear functions such as polynomials or splines for limit surfaces through kernelization by replacing the dot product between two vectors with a more general function [10]. RAVEN can use SVM to construct an initial limit surface, then sample around the surface to refine it [9].

Once a limit surface that separates the input space into safe and unsafe hypergeometries is determined, the unsafe region can be numerically integrated to quantify the probability of failure for a particular accident in the fuel types investigated. The difference between the ATF and oxide failure probabilities directly correlates to the disparity in their unsafe hypervolumes which will yield a benefit CAF if the ATF concept's probability is smaller and a vulnerability if it is larger.

III. RESULTS AND ANALYSIS

1. Nominal Results

Figure 3 presents the axial clad surface temperature at the time of the largest maximum temperature for the silicide and two oxide cases. The oxide case results shown are run at the two different power profiles from Figure 2. The silicide has a higher maximum clad temperature of 1130 K at an earlier

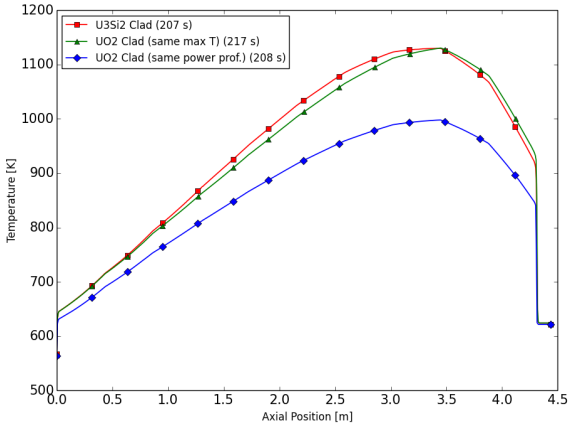

Fig. 3. Axial fuel concept temperature distributions.

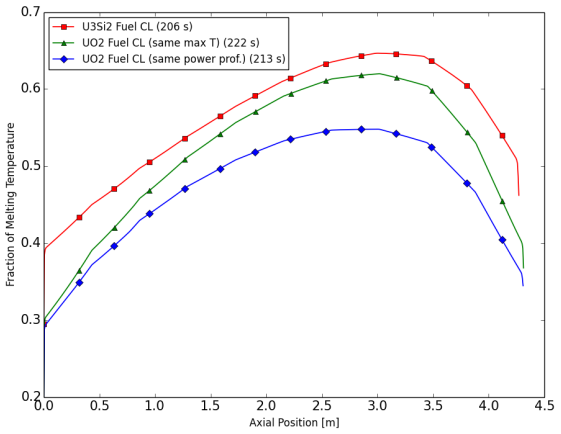

Fig. 4. Axial ratio of fuel centerline temperature to melting temperature.

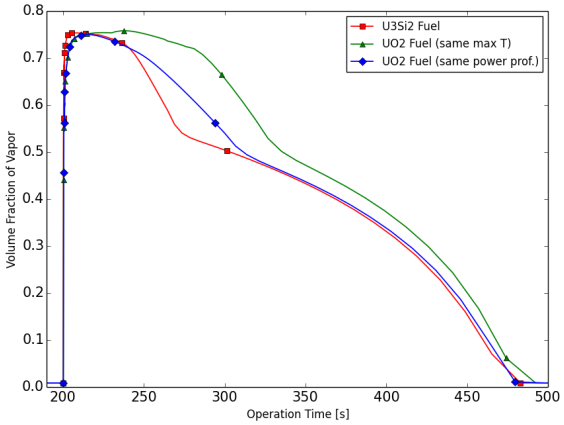

Fig. 5. Volume fraction of vapor at coolant channel outlet over time.

time compared to the oxide fuel which has a maximum surface cladding temperature of 998 K. This result makes sense as the advertised advantage of silicide is the higher heat transfer coefficient, but it does call into question whether an accurate comparison is being drawn between the two fuel systems. The assumption that U_3Si_2 and UO_2 will have the same power profile for the same amount of reactivity being inserted is dubious, but without performing neutronic pin cell calculations to quantify the difference in rod worth, it a fair compromise. However, in order to characterize fuel concept behaviors under similar operational transients, the oxide needs a higher temperature. The power profile is scaled to a larger maximum value with the goal of obtaining a maximum cladding temperature consistent with the silicide case.

The fuel centerline temperature at its largest value for each case can be seen in Figure 4. The temperatures are normalized to each fuel's respective melting temperature (1938 K for silicide and 3138 K in oxide). Silicide is consistently closer to failure when even compared to the higher power profile oxide case, though this maximum is reached much more quickly. Both temperature cases demonstrate that the silicide reaches higher temperatures than the oxide in accident conditions, but it reaches its peak temperature more quickly. The increased heat transfer rate of the silicide could mean the coolant channel spends less time in two phase flow conditions; arguably a more important factor to consider in fuel element failure assessments for RIAs.

A comparison of vapor volume fraction between the silicide and oxide fuel systems at the coolant channel outlet is made in Figure 5. The silicide system boils more quickly than the oxide and at around 250 seconds begins to reduce its volume fraction of vapor more quickly than the oxide. At the same power profile, the silicide takes slightly longer to recover to steady-state single phase flow according to this simulations, but an important factor to keep in mind is that the volume fractions are highly dependent upon the wall heat transfer coefficient between the cladding and coolant. At the moment, single value convective wall heat transfer coefficients are iteratively determined for each case. Only a single H_w value is utilized axially along the fuel element; so these results should be treated as preliminary but do demonstrate general behaviors of the fuel concepts close to when the reactivity insertion accident occurs.

2. Sensitivity Analysis

After perturbing parameters, the largest maximum cladding outer surface temperature obtained is 1146 K and smallest is 1121 K. Results from the oxide case sensitivity analysis are presented in Table II. As a comparison of similar temperature profiles on the clad surface is desired, these and any additional oxide results are generated from the higher power profile oxide case. The least squares fit gives the highest R^2 value, but cross-validated elastic net and cross-validated lasso methods show very similar results. Several unimportant variables have zero coefficients as the L_1 penalty has selected a subset of more sensitive parameters. Also note that the highest L_1 ratio is chosen by the cross validation scheme applied to the elastic net model, giving results as close to the lasso as that

	Least Squares	CV Elastic Net	CV Lasso
R^2	0.99750	0.99748	0.99747
L1 Ratio	-	0.95	(1)
α	-	3.74359×10^{-4}	8.28625×10^{-4}
$p_{\text{liq.,init.}}$	-1.32187e+00	-1.31440e+00	-1.31346e+00
$v_{\text{liq.,init.}}$	1.87986e-04	0.00000e+00	-0.00000e+00
$T_{\text{liq.,init.}}$	2.08947e-02	1.79273e-02	9.83901e-03
ρ_{fuel}	-4.96192e-01	-4.91427e-01	-4.86560e-01
$d_{\text{gap width}}$	2.40889e+00	2.41439e+00	2.41166e+00
$d_{\text{clad thick.}}$	-2.71954e+00	-2.69626e+00	-2.69126e+00
$p_{\text{plen.,init.}}$	1.21873e-01	1.15416e-01	1.09265e-01
R_{clad}	-1.60707e-01	-1.55657e-01	-1.48612e-01
R_{fuel}	-4.65529e-01	-4.59022e-01	-4.52863e-01
$f_{k,\text{fuel}}$	2.83912e+00	2.82547e+00	2.82650e+00
$f_{c_p,\text{fuel}}$	-5.14804e+00	-5.12957e+00	-5.13677e+00
$f_{k,\text{clad}}$	6.04572e-03	7.19987e-04	0.00000e+00

TABLE II. Linear regression model coefficients for high R^2 models for UO_2 normalized using standard deviation (most sensitive parameters are highlighted).

	Least Squares	CV Elastic Net	CV Lasso
R^2	0.99202	0.99199	0.99194
L1 Ratio	-	0.95	(1)
α	-	4.89246×10^{-4}	1.43564×10^{-3}
$p_{\text{liq.,init.}}$	-9.45623e-01	-9.32882e-01	-9.22881e-01
$v_{\text{liq.,init.}}$	-6.41105e-02	-6.12770e-02	-4.04804e-02
$T_{\text{liq.,init.}}$	1.34611e-01	1.28800e-01	1.15525e-01
ρ_{fuel}	-6.61286e-01	-6.51132e-01	-6.38406e-01
$d_{\text{gap width}}$	4.35585e+00	4.34161e+00	4.36625e+00
$d_{\text{clad thick.}}$	-2.88561e+00	-2.87064e+00	-2.82809e+00
$p_{\text{plen.,init.}}$	1.61738e-03	-0.00000e+00	0.00000e+00
R_{clad}	5.84397e-02	4.76140e-02	2.79713e-02
R_{fuel}	2.42991e-01	2.30424e-01	2.15029e-01
$f_{k,\text{fuel}}$	2.05436e-01	1.99115e-01	1.84492e-01
$f_{c_p,\text{fuel}}$	-6.87210e+00	-6.83925e+00	-6.85280e+00
$f_{k,\text{clad}}$	1.43223e-02	1.57040e-02	8.07975e-04

TABLE III. Linear regression model coefficients for high R^2 models for U_3Si_2 normalized using standard deviation (most sensitive parameters are highlighted).

model is allowed. The most sensitive parameters determined by these models are clad thickness, gap width, and scaling factors for specific heat and the heat transfer coefficient.

The maximum surface cladding temperature for the perturbed silicide cases is 1146 K and the minimum is 1117 K; so the silicide has a larger range for this output parameter compared to the oxide. Model characteristics utilized for the sensitivity analysis of the silicide case are found in Table III. The R^2 values for these models are less confident about their predictive capability, but do provide insight into clad temperature sensitivities. Once again, the unpenalized linear least squares model performs better than the shrinkage methods. The three the most sensitive variables (gap width, cladding thickness, and scaling factor of fuel's specific heat) are shared between the silicide and oxide cases, and while the heat transfer coefficient scaling factor is considered a variable of low importance, its strong importance in the oxide case and same order of magnitude with the next most important variable after the three previously discussed allows for its use in the limit surface search.

The extents and sensitivities of the fuel centerline temperature to the perturbed variables was also investigated. The oxide case has maximum and minimum fuel centerline temperatures of 2037 and 1873 respectively. The parameters the centerline temperature is most sensitive to in this case are fuel roughness, fuel k scaling factor, and fuel c_p scaling factor. Perturbations in the maximum fuel centerline temperature of silicide case are more mild with a maximum of 1281 and minimum of 1232. The important parameters of the silicide fuel temperature are fuel roughness, scaling factor of the fuel's specific heat, and the gap width.

3. Limit Surface Search

The limit surface search procedure is a time intensive process. The two fuel system simulations did not converge in time for results to be presented here, but limit surface identification is well on its way to being completed. However, preliminary results generated as the search is in progress can be analyzed. Figure 6 shows the limit surface identified so far with 1140 K as the failure criteria. While there are 663 data points in the visualization, only 458 independent coupled simulations have been run as the SVM reduced order model generates predictions for the surface location. The three spatial dimensions represent gap width, the fuel thermal conductivity scaling factor, and the fuel specific heat scaling factor. The last of the four input variables perturbed is visualized as colormapped data points for the clad thickness. One can see that as this last variable increases in value, the failure surface moves negatively in the gap width and fuel c_p scaling factor spatial dimensions and positively compared to fuel k scaling factor.

Another method of visualizing high dimensional data is demonstrated in Figure 7. Input variable coordinates are normalized on the plot axes and each point identified as lying on either the failure or pass limit surface is plotted as a line. The line color is either blue for passing points or red for failure. The trends identified in the sensitivity analysis are verified here: the fuel specific heat scaling factor has a strongly negative correlation to failure (higher temperatures) while gap width and k scale factor somewhat less strongly correspond to positively to temperature and clad thickness has a negative correlation.

The currently identified limit surface for clad surface maximum temperature of the uranium silicide concept is shown in Figure 8. This surface is generated from the SVM reduced order model utilizing 536 uranium silicide RIA simulation results. This surface has many points sampled on the higher end of the clad thickness input variable's sampling distribution, and appears to have a less regularly predicted structure than the oxide's limit surface. Figure 9 is the parallel coordinates plot of the failure and pass limit surfaces. Again, the predicted sensitivites are evidenced from the failure points' correlation with

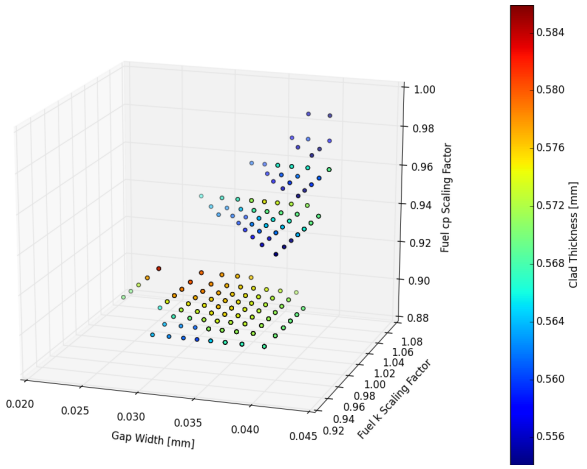

Fig. 6. Visualization of UO_2 failure limit surface.

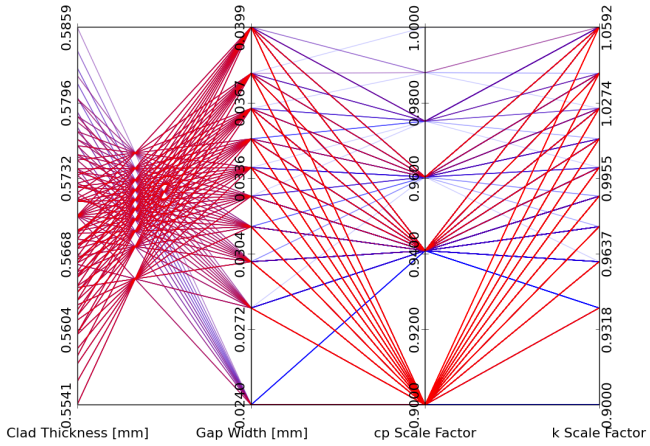

Fig. 7. Parallel coordinates of UO_2 sensitive parameters along limit surface.

the positive or negative sensitivity and sensitivity magnitude.

IV. CONCLUSIONS

By quantifying CAFs using advanced simulation capabilities for use in an existing ATF evaulation framework, potential fuel concepts may be appraised using quantitative metrics. The quantification methodology is not meant to be tied to one tool or analysis method, but as a demonstration of the process to quantify CAFs, the thermal behavior of silicide and oxide fuels are compared during a RIA simulated using coupled BISON and RELAP-7. The results presented illustrate that these codes are capable of running in RIA conditions as well as that sensitivity investigations and limit surface quantification are viable avenues to quantify failure probabilities. In the course of obtaining failure probabilities several vulnerabilities of the silicide concept have been identified including higher fuel and cladding temperatures as well as a lack of information critical to assessing the case (e.g. rod worths of silicide compared to the oxide in RIA conditions, accurate long term two-phase flow results). Converged limit surface run results are forthcoming and a prediction for failure probability can then be made allowing the concept assessment factor to be quantified.

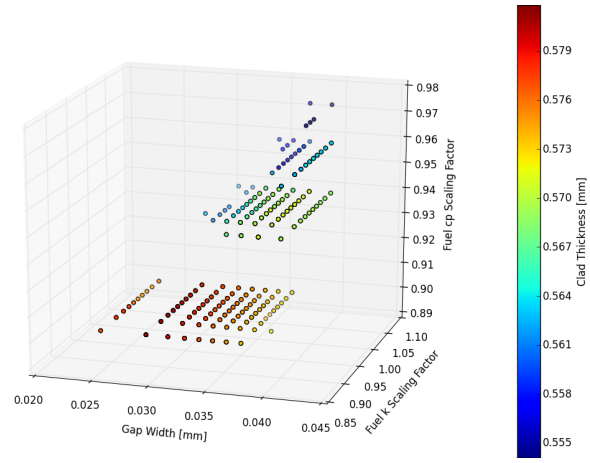

Fig. 8. Visualization of U_3Si_2 failure limit surface.

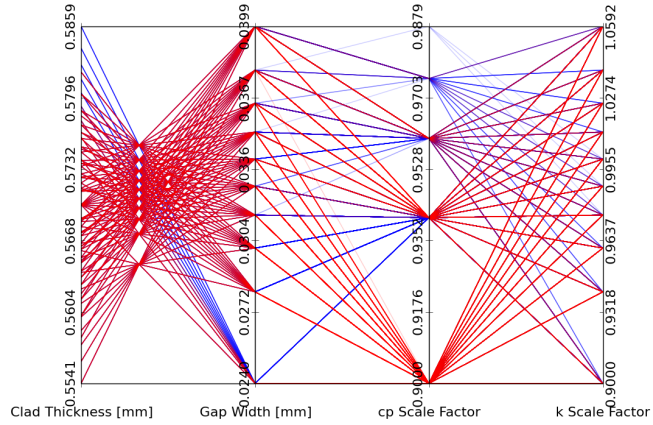

Fig. 9. Parallel coordinates of U_3Si_2 sensitive parameters along limit surface.

V. ACKNOWLEDGMENTS

The phrase, "No man is an island," has never been as evident as in the case of this work. At many points in this project, people offered advice, helped overcome challenges, or suggested a path forward to advance the work. Sincerest thanks go out to everyone named (and unnamed) whose input shaped what was accomplished. Charlie Folsom and Rich Williamson provided excellent resources for getting started in modeling RIAs in BISON, and it was thanks to Al Casagranda alone that patch size issues encountered were diagnosed. Additional BISON troubleshooting and convergence issues were tackled with the aid of Steve Novascone. Without David Andrs, RELAP-7 would not exist as it currently does, and his even-tempered explanations were of great help to the thermo-hydraulically challenged. RAVEN developers continue to be a helpful, enthusiastic team of data minded individuals. Specifically, Cristian Rabiti suggested utilizing RAVEN to compute limit surfaces and calculate failure probailities and Andrea

Alfonsi made these analyses possible through the vast amount of knowledge (not to mention number of merge requests) he has committed to RAVEN. Too many additional smaller contributions were offered to list individually, but thanks go out to the MOOSE team, summer interns, and officemates for all of their expertise, encouragement, and fellowship. The greatest appreciation goes to Jason Hales and Rich Martineau for their mentorship and the opportunity to be part of the great things going on at INL.

REFERENCES

1. C. R. STANEK, "Nuclear Energy Advanced Modeling and Simulation (NEAMS) Program Update," Program Update Presentation (2016).
2. S. M. BRAGG-SITTON, M. TODOSOW, R. MONTGOMERY, ET AL., "Metrics for the Technical Performance Evaluation of Light Water Reactor Accident-Tolerant Fuel," *Nuclear Technology*, **195**, 111–123 (2016).
3. J. D. HALES, W. R. L., S. R. NOVASCONE, ET AL., "BISON Theory Manual," Tech. rep., Idaho National Laboratory (2016).
4. K. J. GEELHOOD, C. E. BEYER, and W. G. LUSCHER, "PNNL Stress/Strain Correlation for Zircaloy," Tech. Rep. PNNL-17700, Pacific Northwest National Laboratory (2008).
5. L. Y. CHENG, A. CUADRA, M. TODOSOW, ET AL., "Performance of U3Si2 Fuel in a Reactivity Insertion Accident," Tech. rep., Brookhaven National Laboratory (2016).
6. O. MARCHAND, J. ZHANG, and M. CHERUBINI, "WGFS RIA Fuels Codes Benchmark Phase-II," Tech. Rep. NEA/CSNI/DOC(2015), Nuclear Energy Agency (2015).
7. J. ORTENSI, F. N. GLEICHER, Y. WANG, ET AL., "MAMMOTH Theory Manual," Tech. rep., Idaho National Laboratory (2016).
8. R. A. BERRY, L. ZOU, H. ZHAO, ET AL., "RELAP-7 Theory Manual," Tech. Rep. INL/EXT-14-31366, Idaho National Laboratory (2014).
9. C. RABITI, A. ALFONSI, J. COGLIATI, ET AL., "RAVEN User Manual," Tech. Rep. INL/EXT-15-34123, Idaho National Laboratory (2016).
10. T. HASTIE, R. TIBSHIRANI, and J. FRIEDMAN, *The Elements of Statistical Learning*, Springer-Verlag, 2nd ed. (2009).
11. M. D. MCKAY, R. J. BECKMAN, and W. J. CONOVER, "A Comparison of Three Methods for Selecting Values of Input Variables in the Analysis of Output from a Computer Code," *Technometrics*, **21**, 239–245 (1979).